Measuring Trotter error and its application to precision-guaranteed Hamiltonian simulations

Tatsuhiko N. Ikeda[1,2,*] Hideki Kono,[3,1,†] and Keisuke Fujii[4,5,1,6,‡]
[1]*RIKEN Center for Quantum Computing, Wako, Saitama 351-0198, Japan*
[2]*Department of Physics, Boston University, Boston, Massachusetts 02215, USA*
[3]*Department of Applied Physics, The University of Tokyo, Hongo, Tokyo 113-8656, Japan*
[4]*Graduate School of Engineering Science, Osaka University, 1-3 Machikaneyama, Toyonaka, Osaka 560-8531, Japan*
[5]*Center for Quantum Information and Quantum Biology, Osaka University, Osaka 560-0043, Japan*
[6]*Fujitsu Quantum Computing Joint Research Division at QIQB, Osaka University, 1-2 Machikaneyama, Toyonaka 560-0043, Japan*

(Received 13 July 2023; accepted 24 August 2024; published 12 September 2024)

Trotterization is the most common and convenient approximation method for Hamiltonian simulations on digital quantum computers, but estimating its error accurately is computationally difficult for large quantum systems. Here, we develop a method for measuring the Trotter error without ancillary qubits on quantum circuits by combining the mth- and nth-order ($m < n$) Trotterizations rather than consulting with mathematical error bounds. Using this method, we make Trotterization precision guaranteed, developing an algorithm named Trotter(m, n), in which the Trotter error at each time step is within an error tolerance ϵ preset for our purpose. Trotter(m, n) is applicable to both time-independent and -dependent Hamiltonians, and it adaptively chooses almost the largest step size δt, which keeps quantum circuits shallowest, within the error tolerance. Benchmarking it in a quantum spin chain, we find the adaptively chosen δt to be about 10 times larger than that inferred from known upper bounds of Trotter errors.

DOI: 10.1103/PhysRevResearch.6.033285

I. INTRODUCTION

The rapid development of quantum devices in recent years has led researchers to find useful applications with significant quantum advantage [1–3]. On top of the eigenvalue problems [4–9], quantum many-body dynamics, or Hamiltonian simulation [10–15], is one of the most promising candidates because quantum computers could overcome the exponential complexity that classical computers face [5], enabling us to address intriguing dynamical phenomena like nonequilibrium phases of matter [16–19] and to implement fundamental quantum algorithms like phase estimation [20]. Among several algorithms for the Hamiltonian simulation, Trotterization [21,22] is and will be used most commonly in the current noisy intermediate-scale quantum (NISQ [23]) era and the coming early fault-tolerant quantum computing (FTQC) era because it does not demand additional ancillary qubits or largely controlled quantum gates. Indeed, quantum advantage in Trotterized dynamics simulation has been reported using a 127-qubit NISQ computer only recently [24].

One major and presumably inevitable issue of Trotterization is the tradeoff relation between the simulation accuracy and the circuit depth (see, however, Refs. [25–30] for variational approaches). The kth-order Trotterization accompanies an error of $O(\delta t^{k+1})$ during a single time step δt, which decreases when δt is taken shorter. In the meantime, the number of steps to reach a final time increases, meaning a deeper quantum circuit. To suppress the gate depth, it is desirable to choose the largest possible step size δt, i.e., the shallowest circuit, within our error tolerance ϵ preset for our purposes.

However, it is difficult to find the optimal step size δt because the Trotter error is complex in generic many-body systems. According to the previous studies on the Trotter error, its upper bounds [31,32] and typical values [33] are available. If we choose δt so that the upper bound is below our tolerance ϵ, the precision is guaranteed, but δt tends to be too small, as we will see below. On the other hand, if we choose δt based on the typical values, δt can be larger, but the precision guarantee is lost. Recently, Zhao *et al.* [34] proposed an approach where δt is chosen adaptively in each time step based on the energy expectation value and variance. Yet, the precision guarantee of this method is still elusive, and the applicability is limited to time-independent Hamiltonians [35].

In this paper, we develop a method to measure the Trotter error on quantum circuits by combining Trotterization formulas at different orders, m and $n(> m)$. Since measured, the estimated error is significantly more accurate than known upper bounds for it and thus allows us to accurately choose the largest possible step size δt so that the error does not exceed our tolerance ϵ. Using this method, we make Trotterization precision guaranteed, in which almost the largest δt is adaptively chosen within a preset error tolerance ϵ (see

*Contact author: tatsuhiko.ikeda@riken.jp
†Contact author: konofr0924@g.ecc.u-tokyo.ac.jp
‡Contact author: keisuke.fujii.ay@riken.jp

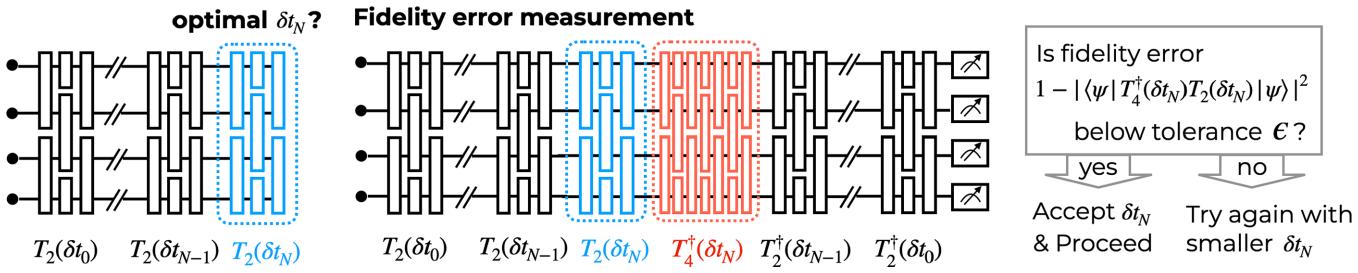

FIG. 1. Key concept of (fidelity-based) Trotter24. (Left) At each time step N, we ask what the optimal step size δt_N for the second-order Trotterization formula $T_2(\delta t_N)$. Here the optimal means the largest with the fidelity error kept less than our tolerance ϵ. (Middle) The fidelity error that $T_2(\delta t_N)$ can be measured using the fourth-order Trotterization $T_4(\delta t_N)$, instead of the exact evolution $U(\delta t_N)$ when we neglect higher-order corrections in terms of δt_N. (Right) If the measured error is below our tolerance, we accept the value of δt_N and proceed to the next time step $N+1$. Otherwise, we reject the value and try the same protocol with a smaller value for δt_N again. In the paper, we also develop an observable-based, rather than fidelity-based, algorithm, establish an efficient scheme for avoiding the possible rejections of δt_N's, and analyze how errors propagate with time steps.

Fig. 1 for its structure). We name this algorithm Trotter (m, n) in analogy to RFK45 (Runge-Kutta-Fehlberg) for classical simulations, where the fourth- and fifth-order methods are combined. We benchmark Trotter24 in a quantum spin chain under time-independent and -dependent Hamiltonians, finding that the adaptively chosen δt is about 10 times larger than that inferred from the upper bound of Trotter errors.

II. MEASURING TROTTER ERROR

In this section, we present a way to measure a Trotter error on quantum circuits without ancillary qubits when a quantum state is evolved by an mth order Trotterization for a small time step δt. A key idea is making use of a higher-order $n(>m)$th Trotterization to approximate the unknown exact solution accurately enough.

A. Extracting Trotter error using different orders

For simplicity, we first consider a time-independent Hamiltonian H consisting of two parts,

$$H = A + B, \tag{1}$$

where A and B do not necessarily commute with each other. Generalization to more noncommuting parts is straightforward, and we will generalize the arguments to time-dependent ones later in Sec. VI. We assume that the quantum state at time t is known to be $|\psi(t)\rangle$ and consider evolving it by a small time step δt,

$$|\psi(t+\delta t)\rangle = U(\delta t)\,|\psi(t)\rangle = e^{-iH\delta t}\,|\psi(t)\rangle\,. \tag{2}$$

Trotterization approximately decomposes $e^{-iH\delta t}$ into quantum-gate-friendly parts consisting of either A and B. We take an mth-order Trotterization $T_m(\delta t)$. For example, $T_m(\delta t)$ can be the Lie-Trotter formula $T_1(\delta t) = e^{-iA\delta t}e^{-iB\delta t}$ for $m=1$ or its symmetrized form $T_2(\delta t) \equiv e^{-iA\delta t/2}e^{-iB\delta t}e^{-iA\delta t/2}$ for $m=2$. In general, $T_m(\delta t)$ approximates $U(\delta t)$ up to the order of δt^m and satisfies

$$T_m(\delta t) = e^{-iH\delta t+\Upsilon_{m+1}}, \tag{3}$$

where $\Upsilon_{m+1} = O(\delta t^{m+1})$ is an anti-Hermitian error operator. These relations imply

$$|\psi_m(t+\delta t)\rangle \equiv T_m(\delta t)\,|\psi(t)\rangle = |\psi(t+\delta t)\rangle + O(\delta t^{m+1}), \tag{4}$$

meaning that $T_m(\delta t)$ approximates the exact one-step evolution within an error of $O(\delta t^{m+1})$.

To quantify the error arising in the one step, we adopt the square root of the infidelity

$$\eta_F \equiv \sqrt{1-|\langle\psi(t+\delta t)|\psi_m(t+\delta t)\rangle|^2}. \tag{5}$$

We can also use other quantities depending on our purposes and make parallel arguments. For example, when we are interested in the expectation value of an observable O, we care about the error in it,

$$\eta_O \equiv \langle\psi(t+\delta t)|O|\psi(t+\delta t)\rangle - \langle\psi_m(t+\delta t)|O|\psi_m(t+\delta t)\rangle. \tag{6}$$

In either case, calculating η_F or η_O is difficult because we do not know the exactly evolved state $|\psi(t+\delta t)\rangle$.

We remark that both η_F and η_O are $O(\delta t^{m+1})$, but showing $\eta_F = O(\delta t^{m+1})$ is less obvious. To show this, we note that the leading $O(\delta t^{m+1})$ term of $1-\langle\psi(t+\delta t)|\psi_m(t+\delta t)\rangle$ is pure imaginary as shown in Appendix A, and its leading-order contribution of η_F is given by

$$\eta_F = \sqrt{\langle\psi(t)|(i\Upsilon_{m+1})^2|\psi(t)\rangle - \langle\psi(t)|(i\Upsilon_{m+1})|\psi(t)\rangle^2} + O(\delta t^{m+2}), \tag{7}$$

where $i\Upsilon_{m+1}$ is Hermitian. Equation (7) dictates that η_F is the variance of the "observable" $i\Upsilon_{m+1}$, giving a way to estimate η_F using $|\psi(t)\rangle$ and the explicit form of $i\Upsilon_{m+1}$. Indeed this is a possible way of measuring η_F, but it requires, for generic many-body Hamiltonians, measuring numerous Hermitian operators involved in $i\Upsilon_{m+1}$ consisting of doubly nested commutators between A and B. Hence, in the following subsection, we will also discuss another way to estimate η_F with less sampling costs.

Our idea of estimating the errors is the following: In calculating η_F and η_O in the leading order, we can safely replace the exact $|\psi(t+\delta t)\rangle$ by a higher-order approximant $|\psi_n(t+\delta t)\rangle$

for $n > m$. Replacing $|\psi(t+\delta t)\rangle$ by $|\psi_n(t+\delta t)\rangle$ in η_F and η_O, we obtain the following key analytical results (see Appendix A for derivation): For the fidelity error,

$$\eta_F = \eta_F^{(mn)} + O(\delta t^{n+1}), \tag{8}$$

$$\eta_F^{(mn)} \equiv \sqrt{1 - |\langle\psi_n(t+\delta t)|\psi_m(t+\delta t)\rangle|^2}, \tag{9}$$

and, for the observable error,

$$\eta_O = \eta_O^{(mn)} + O(\delta t^{n+1}), \tag{10}$$

$$\eta_O^{(mn)} \equiv \langle\psi_n(t+\delta t)|O|\psi_n(t+\delta t)\rangle - \langle\psi_m(t+\delta t)|O|\psi_m(t+\delta t)\rangle\,. \tag{11}$$

Given that $\eta_F = O(\delta t^{m+1})$ and $\eta_O = O(\delta t^{m+1})$, these results mean that $\eta_F^{(mn)}$ ($\eta_O^{(mn)}$) coincides with η_F (η_O) in the leading order since $m < n$. If $n \leqslant m$, the above equations hold true, but $O(\delta t^{n+1})$ contributions are non-negligible, and $\eta^{(mn)}$ do not give good estimates for η.

Unlike η_F and η_O, $\eta_F^{(mn)}$ and $\eta_O^{(mn)}$ consist of $T_m(\delta t)$ and $T_n(\delta t)$ and are thereby implementable in quantum circuits. In other words, we can estimate the deviation from the exact solution induced by $T_m(\delta t)$ without knowing the solution when supplemented with the fourth-order Trotterization and neglect higher-order corrections. We will discuss in more detail how to measure $\eta_F^{(mn)}$ and $\eta_O^{(mn)}$ in Sec. II B.

We emphasize that η_F and η_O are the actual Trotter error specific to the current state $|\psi(t)\rangle$. This contrasts the upper-bound arguments on the operator difference $U(\delta t) - T_m(\delta t)$ [31,32]. Such upper bounds apply to arbitrary states and are thus always larger than or equal to the error occurring at a specific state $|\psi(t)\rangle$. The fact that η_F and η_O are state dependent enables us to choose δt more accurately so that the error is below our tolerance, as we will see in detail below.

We highlight two sets of (m, n) of particular interest in practical use. The first choice is the minimum pair $(m, n) = (1, 2)$, for which the Trotterizations T_m and T_n involve the minimum possible exponentials, i.e., the gate complexity in the quantum circuit. For noisy circuits, such lowest-order Trotterizations are commonly used to avoid gate errors as much as possible. The second choice is the pair of minimum even numbers $(m, n) = (2, 4)$, which can be useful when we can use more gates to achieve higher accuracy. Changing m from 1 to 2 increases the number of exponentials in T_m from 2 to 3, by which the Trotter error η_F or η_O becomes one order smaller. In this case, using $n = 4$ rather than $n = 3$ could be beneficial. To see this, let us compare Ruth's third-order formula [22,36]

$$T_3(\delta t) \equiv e^{-i\frac{7}{24}A\delta t} e^{-i\frac{2}{3}B\delta t} e^{-i\frac{3}{4}A\delta t} e^{i\frac{2}{3}B\delta t} e^{i\frac{1}{24}A\delta t} e^{-iB\delta t} \tag{12}$$

and the fourth-order Forest-Ruth-Suzuki (FRS) formula [37,38]

$$T_4(\delta t) \equiv e^{-i\frac{s}{2}A\delta t} e^{-isB\delta t} e^{-i\frac{1-s}{2}A\delta t} e^{-i(1-2s)B\delta t} \times e^{-i\frac{1-s}{2}A\delta t} e^{-isB\delta t} e^{-i\frac{s}{2}A\delta t}, \tag{13}$$

where $s = (2 - 2^{1/3})^{-1}$. Here we note that the FRS formula involves only one extra exponential but is one order more accurate than Ruth's third-order formula. Since $\eta^{(24)}$ estimates $\eta^{(23)}$ one order more accurately at the expense of an extra exponential, it can be worth using $n = 4$ for $m = 2$.

B. Quantum circuit implementations

In Sec. II A we derived two expressions, Eqs. (7) and (8), for estimating the fidelity error η_F and one (10) for the observable error η_O. We are assuming a quantum advantage regime, where the number of qubits is so large that $|\psi(t)\rangle$ cannot be stored in classical computer memory but is realized on a quantum circuit. In such a regime, all the expressions for η_F and η_O cannot be evaluated with classical linear algebraic computations, and we need to develop ways to evaluate them on quantum circuits.

First, let us consider how to measure the leading-order contribution in Eq. (7) of the fidelity error η_F, assuming that $|\psi(t)\rangle$ is realized on a quantum circuit accurately enough. For concreteness we focus on the first-order Trotterization $m = 1$, for which $T_1(\delta t) = e^{-iA\delta t} e^{-iB\delta t}$ and $i\Upsilon_2 = -i[A, B]\delta t^2$. Since $i\Upsilon_2$ and $(i\Upsilon_2)^2$ are Hermitian, one can evaluate the expectation values for them based on samplings (we will discuss the sampling cost below).

Although this method is useful for small quantum systems, it becomes quadratically costly for larger systems. To see this we consider a Hamiltonian H with A and B are linear combinations of L distinct local Pauli strings. Thanks to the commutator scaling [32], $i\Upsilon_2$ consists of $O(L)$ distinct Pauli strings, and its expectation values are evaluated by estimating the expectation values of each Pauli string. Notably, the translation symmetries can reduce the number of combinations of measurements for expectation value estimations, even down to $O(1)$. However, $(i\Upsilon_2)^2$ is no more a commutator and involves $O(L^2)$ Pauli strings. In most cases symmetries cannot reduce the number of measured operators to be subextensive, and the sampling cost tends to be extensive. This extensive sampling cost also appears in the energy variance estimation in Refs. [34,39]. Thus, Eq. (7) tends to be useful only in small quantum systems.

In contrast, $\eta_F^{(mn)}$ in Eq. (8) avoids measuring numerous distinct Pauli strings. To show this we write $|\psi(t)\rangle$ as $|\psi(t)\rangle = U_T(t)\,|\psi(0)\rangle = U_T(t)U_{\rm prep}\,|\mathbf{0}\rangle$. Here $|\mathbf{0}\rangle$ denotes the initialized state, $U_{\rm prep}$ is an initial state preparation unitary, and $U_T(t)$ is some Trotterized unitary propagation from time 0 to t. We assume $U_{\rm prep}$ and $U_T(t)$ have appropriate circuit realizations. With these notations $\eta_F^{(mn)}$ can be obtained by

$$\eta_F^{(mn)} = \sqrt{1 - p_{\mathbf{0}}}, \tag{14}$$

$$p_{\mathbf{0}} \equiv |\langle\mathbf{0}|U_{\rm prep}^\dagger U_T^\dagger(t) T_n^\dagger(\delta t) T_m(\delta t) U_T(t)|\mathbf{0}\rangle|^2. \tag{15}$$

Our assumptions tell us that $U_{\rm prep}^\dagger U_T^\dagger(t) T_n^\dagger(\delta t) T_m(\delta t) U_T(t)$ has a circuit realization, so $p_{\mathbf{0}}$ can be interpreted by the probability of finding $|\mathbf{0}\rangle$ after $|\mathbf{0}\rangle$ being evolved by the circuit (see also the middle panel of Fig. 1). Note that $p_{\mathbf{0}}$ is a kind of the Loschmidt echo [40]. A challenge is that $p_{\mathbf{0}}$ becomes exponentially small when the system size L increases, so this procedure makes practical sense only in small systems. This issue is not technical but intrinsic in the fidelity error because it is the most stringent quantifier among many-body wave-function errors.

The observable error η_O is more useful for extensive quantum systems. Typically we are interested in local Pauli strings or their linear combinations of $O(L)$. The expectation value of each Pauli string can be estimated by measuring the wave function $|\psi(t)\rangle$ in its eigenbasis. Unlike fidelity, the expectation value does not decay exponentially with the system size. Also, symmetries, such as the translation one, can reduce the number of measured strings to possibly $O(1)$. When one is only interested in local observables, using η_O is the cheapest option to guarantee precision.

In each method, the Trotter error estimation is based on sampling, and the statistical error can be a bottleneck to achieve high accuracy. The statistical error in general scales as $\propto \mathcal{N}^{-1/2}$, with $\mathcal{N}$ denoting the number of samples (or shots). For the error estimation to be successful, this error should be smaller enough than the error, η_F or η_O, so $\delta t^{m+1} \gtrsim \mathcal{N}^{-1/2}$ must hold true. When we use $\eta^{(mn)}$ as an estimator, the estimation error is determined by the larger of $\sim\mathcal{N}^{-1/2}$ and $\sim\delta t^{n+1}$ [see Eqs. (8) and (10)]. So, one cannot make the error estimation infinitely accurate by increasing n when the available number of shots $\mathcal{N}$ is limited finitely. Rather, $\delta t^{n+1} \sim \mathcal{N}^{-1/2}$ would hold for a reasonably chosen set of δt, n, and $\mathcal{N}$. In Sec. V B, we will benchmark our way to estimate η_O for $(m, n) = (2, 4)$ in an example spin system and show that it works with $\mathcal{N} \sim 10^5(10^7)$ for $\epsilon_O = 10^{-2}(10^{-3})$.

III. PRECISION-GUARANTEED TROTTERIZATION

In the previous section, we developed the methods to evaluate Trotter errors on quantum circuits. Given that the Trotter error is known, one can make Trotterization precision guaranteed: In each time step, one can make sure that the Trotter error is within a preset accuracy target ϵ. In this section we develop such an algorithm consisting of error measurements and step-size optimization, as illustrated in Fig. 1 (the figure is for the fidelity version, but it works, in parallel, for the observable version).

Our algorithm uses either $\eta_F^{(mn)}$ and $\eta_O^{(mn)}$ as the Trotter error estimator, and we name it Trotter(m, n). For concreteness we set $(m, n) = (2, 4)$ and describe Trotter24 since the generalization to other (m, n) is straightforward [we may use Trotter(m, n) and Trottermn interchangeably]. In current NISQ devices, $(m, n) = (1, 2)$ could be more realistic. Since the argument goes in parallel, we first focus on the fidelity error and will address the observable error later in this section.

Our overall task is to simulate the time evolution according to the Hamiltonian H from the initial time $t_{\rm ini}$ to the final time $t_{\rm fin}$, starting from an initial state $|\psi_0\rangle$. We set an error tolerance ϵ for the fidelity error in each time step. Initially, we have no *a priori* information about the appropriate time step, so take a reasonably small trial step size δt_0, say, $\delta t_0 = 0.1J^{-1}$ with J being a typical energy scale of H. One could also choose δt_0 so small that $T_2(\delta t_0)$ never gives larger error than our tolerance ϵ, as guaranteed by a mathematical bound [see Eq. (29) and Appendix C for detail]. One can also use this δt_0 to know the upper bound, in advance, for the required quantum resources for the calculation, although they tend to be too pessimistic, as we will see below.

For the trial δt_0 taken in either way, we implement $T_2(\delta t_0)$ and $T_4(\delta t_0)$ and calculate $\eta_F^{(24)}$ using a quantum circuit. Basically, we aim the step size to be so small that

$$\eta_F^{(24)} < \epsilon. \tag{16}$$

If this is true, we accept our trial δt_0 and evolve our state as $|\psi_2\rangle = T_2(\delta t_0)|\psi_0\rangle$. If $\eta_F^{(24)} \geqslant \epsilon$ instead, our trial δt_0 is too large and we need a smaller $\delta t_0'$. In choosing $\delta t_0'$ appropriately, we invoke the leading-order scaling relation $\eta_F^{(24)} \approx \alpha \delta t_0^3$ for some unknown α independent of δt_0. We can use this relation to estimate α by $\alpha \approx \eta_F^{(24)}/\delta t_0^3$ since we measured $\eta_F^{(24)}$. For $\delta t_0'$, we expect $\eta_F^{(24)\prime} \approx \alpha(\delta t_0')^3 \approx \eta_F^{(24)}(\delta t_0'/\delta t_0)^3$, which we wish is smaller than ϵ. Thus, the condition $\eta_F^{(24)\prime} < \epsilon$ leads to $\delta t_0' \approx \delta t_0(\epsilon/\eta_F^{(24)})^{1/3}$ as an optimal choice within our error tolerance. For a safety margin, we introduce a constant C $(0 < C < 1)$ and set $\delta t_0' = C\delta t_0(\epsilon/\eta_F^{(24)})^{1/3}$ as an updated trial δt_0. We repeat this update procedure until $\eta_F^{(24)}$ gets smaller than ϵ and accept the latest δt_0 to evolve our state as $|\psi_2\rangle = T_2(\delta t_0)|\psi_0\rangle$.

Next, we move on to the second step, using a time step δt_1. In choosing this, we again use the latest $\eta_F^{(24)}$ obtained at the end of the previous time step. Since $|\psi_2\rangle \approx |\psi_0\rangle$, we can expect the error scaling coefficient α to be almost the same in the present and previous steps. Therefore, like in the updated trials within the previous time step, we have $\delta t_1 = C\delta t_0(\epsilon/\eta_F^{(24)})^{1/3}$ as a good candidate for the optimal step size in the present time step. We note that $\eta_F^{(24)}$ here is what was measured in the previous step, and we have not made any measurements in the present step yet. Using this δt_1 as a trial step size, we implement $T_2(\delta t_1)$ and $T_4(\delta t_1)$ and calculate $\eta_F^{(24)}$ using a quantum circuit. Depending on whether $\eta_F^{(24)}$ is less or greater than ϵ, we accept or update δt_1 like in the previous step.

The following iteration is straightforward and repeated until the accumulated evolution time $t_{\rm ini} + \delta t_0 + \delta t_1 + \cdots$ exceeds the final time $t_{\rm fin}$. We summarize a pseudocode for the algorithm in Algorithm 1.

Let us make a parallel argument for the observable error η_O instead of the fidelity error η_F. At each time step, we measure $\eta_O^{(24)}$ and judge if the condition

$$\left|\eta_O^{(24)}\right| < \epsilon_O \|O\| \tag{17}$$

is met. This is an analog of Eq. (16), and we introduced the operator norm $\|O\|$ as a reference scale and put the subscript O on the tolerance as ϵ_O to avoid confusion. The iteration scheme is parallel to the fidelity case. We summarize a pseudocode for the observable-based algorithm in Algorithm 2.

IV. ERROR PROPAGATION

In this section we analyze the fidelity and observable Trotter errors in multiple Trotter steps, showing that both errors increase at most linearly in the number of steps. For generality we consider an mth-order Trotterization, which was set to be $m = 2$ in the previous section.

After N $(\geqslant 1)$ steps, we obtain a quantum state

$$|\psi_m(t_N)\rangle = \overleftarrow{\prod_{i=0,\ldots,N-1}} T_m(\delta t_i)|\psi_0\rangle \tag{18}$$

ALGORITHM 1. Fidelity-based Trotter24.

Input: Initial and final times, $t_{\rm ini}$ and $t_{\rm fin}$, an initial state $|\psi_0\rangle$, a Hamiltonian $H = A + B$, an error tolerance ϵ, an initial step size δt_0, a safety constant C $(0 < C < 1)$, an oracle function FIDELITY$(|\phi\rangle, |\psi\rangle)$ that calculates $|\langle\phi|\psi\rangle|^2$.
Output: An ordered list of unitaries $U_{\rm list}$ that approximates $e^{-iH(t_{\rm fin}-t_{\rm ini})}$ within the error tolerance for each time step.

$t \leftarrow t_{\rm ini}$
$\delta t \leftarrow \delta t_0$
$U_{\rm list} = \{\}$ (empty list)
while $t + \delta t < t_{\rm fin}$ **do**
  $|\psi(t)\rangle \leftarrow \prod_k (U_{\rm list})_k |\psi_0\rangle$
  do
    $T_2(\delta t) \leftarrow e^{-iA\delta t/2} e^{-iB\delta t} e^{-iA\delta t/2}$
    $T_4(\delta t) \leftarrow e^{-i\frac{s}{2}A\delta t}\, e^{-isB\delta t}\, e^{-i\frac{1-s}{2}A\delta t}\, e^{-i(1-2s)B\delta t} e^{-i\frac{1-s}{2}A\delta t}\, e^{-isB\delta t}\, e^{-i\frac{s}{2}A\delta t}$
    $\eta \leftarrow 1 - \text{FIDELITY}(T_4(\delta t)|\psi(t)\rangle, T_2(\delta t)|\psi(t)\rangle)$
    $\delta t \leftarrow C \cdot (\epsilon/\eta)^{1/3}\delta t$
  while $\eta > \epsilon$
  Prepend $T_2(\delta t)$ to the ordered list $U_{\rm list}$
  $t \leftarrow t + \delta t$
return $U_{\rm list}$

at time

$$t_N = t_{\rm ini} + \sum_{i=0}^{N-1} \delta t_i \tag{19}$$

as an approximation for the exact state

$$|\psi(t_N)\rangle = \overleftarrow{\prod_{i=0,\ldots,N-1}} U(\delta t_i)|\psi_0\rangle = e^{-iH(t_N - t_{\rm ini})}|\psi_0\rangle . \tag{20}$$

ALGORITHM 2. Observable-based Trotter24.

Input: Initial and final times, $t_{\rm ini}$ and $t_{\rm fin}$, an initial state $|\psi_0\rangle$, a Hamiltonian $H = A + B$, an error tolerance ϵ_O, an initial step size δt_0, a safety constant C $(0 < C < 1)$, an oracle function EXP$(O, |\psi\rangle)$ that calculates $\langle\psi|O|\psi\rangle$.
Output: An ordered list of unitaries $U_{\rm list}$ that approximates $e^{-iH(t_{\rm fin}-t_{\rm ini})}$ within the error tolerance for each time step.

$t \leftarrow t_{\rm ini}$
$\delta t \leftarrow \delta t_0$
$U_{\rm list} = \{\}$ (empty list)
while $t + \delta t < t_{\rm fin}$ **do**
  $|\psi(t)\rangle \leftarrow \prod_k (U_{\rm list})_k |\psi_0\rangle$
  do
    $T_2(\delta t) \leftarrow e^{-iA\delta t/2} e^{-iB\delta t} e^{-iA\delta t/2}$
    $|\psi_2\rangle \leftarrow T_2(\delta t)|\psi(t)\rangle$
    $T_4(\delta t) \leftarrow e^{-i\frac{s}{2}A\delta t}\, e^{-isB\delta t}\, e^{-i\frac{1-s}{2}A\delta t}\, e^{-i(1-2s)B\delta t} \times e^{-i\frac{1-s}{2}A\delta t}\, e^{-isB\delta t}\, e^{-i\frac{s}{2}A\delta t}$
    $|\psi_4\rangle \leftarrow T_4(\delta t)|\psi(t)\rangle$
    $\eta \leftarrow |\text{EXP}(O, |\psi_4\rangle) - \text{EXP}(O, |\psi_2\rangle)|$
    $\delta t \leftarrow C \cdot (\epsilon/\eta)^{1/3}\delta t$
  while $|\eta| > \epsilon_O \|O\|$
  Prepend $T_2(\delta t)$ to the ordered list $U_{\rm list}$
  $t \leftarrow t + \delta t$
return $U_{\rm list}$

This section gives upper bounds for accumulated errors in the N steps. As expected, we will have error propagation linear in N. Throughout this section, we let $\sim$ and $\lesssim$ denote $=$ and $\leqslant$, respectively, when subleading terms in δt_j $(j = 0, \ldots, N-1)$ are neglected.

For the fidelity-based Trotter(m, n), let us find an upper bound for the accumulated error

$$\eta_{F,N} \equiv \sqrt{1 - |\langle\psi(t_N)|\psi_m(t_N)\rangle|^2}. \tag{21}$$

As we derive in Appendix B,

$$\eta_{F,N} \lesssim N\epsilon, \tag{22}$$

meaning a linear increase in the fidelity error. This upper bound implies an upper bound for the error in the expectation value of an arbitrary observable O,

$$\eta_{O,N} \equiv |\langle\psi(t_N)|O|\psi(t_N)\rangle - \langle\psi_m(t_N)|O|\psi_m(t_N)\rangle|. \tag{23}$$

To derive the bound for $\eta_{O,N}$, we recall $\eta_{O,N} \leqslant 2D(|\psi(t_N)\rangle\langle\psi(t_N)|, |\psi_m(t_N)\rangle\langle\psi_m(t_N)|)\|O\|$, where $D(\rho, \sigma)$ denotes the trace distance, which is known to satisfy $D(\rho, \sigma) \leqslant \sqrt{1 - F(\rho, \sigma)}$ with $F(\rho, \sigma)$ being the fidelity. Using Eq. (22), we obtain

$$\eta_{O,N} \lesssim N\epsilon\|O\|, \tag{24}$$

which linearly increases with N.

For the observable-based Trotter(m, n) using an observable O, let us find an upper bound with the tolerance ϵ_O for the accumulated error (23) arising in the same observable. We can prove

$$\eta_{O,N} \lesssim N\epsilon_O\|O\| \tag{25}$$

by induction on N. This claim trivially holds when $N = 1$ by the definition of δt_0. Suppose that Eq. (25) for N. For $N + 1$, the triangle inequality gives

$$\begin{aligned}\eta_{O,N+1} \leqslant\ & |\langle\psi(t_{N+1})|O|\psi(t_{N+1})\rangle \\ & - \langle\psi_m(t_N)|U^\dagger(\delta t_N)OU(\delta t_N)|\psi(t_N)\rangle| \\ & + |\langle\psi_m(t_N)|U^\dagger(\delta t_N)OU(\delta t_N)|\psi(t_N)\rangle \\ & - \langle\psi_m(t_{N+1})|O|\psi_m(t_{N+1})\rangle|. \end{aligned} \tag{26}$$

Since $U^\dagger(\delta t_N)OU(\delta t_N) \sim O$, the first term on the right-hand side is $\lesssim N\epsilon_O\|O\|$ by the inductive hypothesis. The second term on the right-hand side is less than $\epsilon_O\|O\|$, as implemented in the algorithm. Combining these two, we obtain $\eta_{O,N+1} \lesssim (N+1)\epsilon_O\|O\|$, which completes the induction.

V. BENCHMARK IMPLEMENTATIONS

In this section we implement and benchmark Trotter(m, n), using a classical computer. In the first subsection we consider the ideal limit of the infinite number of shots, for which the error estimators $\eta_F^{(mn)}$ and $\eta_O^{(mn)}$ can be obtained without statistical errors. Then, in the second subsection, we discuss a more realistic situation, where the number of shots is limited to be finite. In both subsections we neglect errors in the quantum circuit.

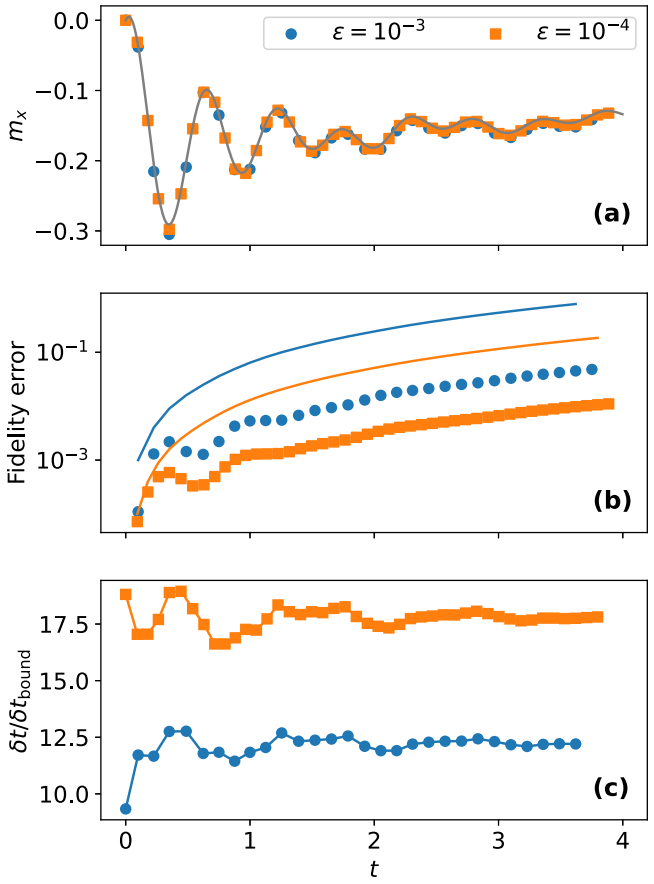

FIG. 2. (a) Dynamics of x-magnetization density calculated by fidelity-based Trotter24 for tolerance $\epsilon = 10^{-3/2}$ (circle) and 10^{-2} (square). The solid curve shows the accurate solution, the system size is $L = 18$, and the safety constant is $C = 0.95$. (b) The actual fidelity errors η_F [Eq. (5)] in the simulation presented in (a). The solid curves show their upper bounds (22). Blue (orange) points and curve correspond to the case of $\epsilon = 10^{-3/2}$ (10^{-2}). (c) The ratio of the step size δt chosen in each step to $\delta t_{\rm bound}$ obtained by the error-bound approach (29). Different symbols correspond to those in (a).

A. Ideal limit of $\mathcal{N}_{\rm shots} = \infty$

First, we implement the fidelity-based Trotter24 and will address the observable-based one later in this section. In both cases we assume that both $\eta_F^{(mn)}$ and $\eta_O^{(mn)}$ can be obtained without statistical errors. Following Ref. [34], we consider the following Hamiltonian:

$$A = h_x \sum_{j=1}^{L} \sigma_j^x, \quad B = \sum_{j=1}^{L} \left(J_z \sigma_j^z \sigma_{j+1}^z + h_z \sigma_j^z \right), \tag{27}$$

where σ_j^α are the Pauli matrices acting on the jth site, periodic boundary conditions are imposed, and we set $J_z = -1.0$, $h_z = 0.2$, and $h_x = -2.0$. Taking the initial state fully polarized along the $-y$ direction, we let it evolve for a while. Figure 2(a) shows the expectation value of the x-magnetization density

$$m_x \equiv \frac{1}{L} \sum_{j=1}^{L} \sigma_j^x \tag{28}$$

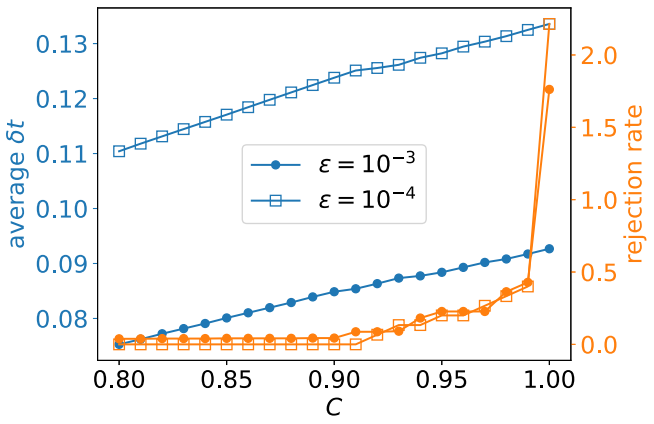

FIG. 3. The C dependence of the average step size δt (left y axis) and the rejection rate (right y axis), i.e., the occurrence of $\eta_F^{(24)} > \epsilon$ per time step. Different symbols correspond to $\epsilon = 10^{-3/2}$ (circle) and 10^{-2} (square). The averages are taken for $t_{\rm ini} = 0.0$ and $t_{\rm fin} = 2.0$ with the initial trial step size $\delta t_0 = 0.1$.

for different tolerances $\epsilon = 10^{-3/2}$ and 10^{-2} at $L = 18$, and we set $C = 0.95$. As expected, for smaller tolerance, the simulated dynamics resemble the exact result better, as shown in the upper panel. We note that we encounter few $\eta^{(24)} > \epsilon$ in these simulations: it happens three (five) times for $\epsilon = 10^{-3/2}$ (10^{-2}) during the simulation time range. These numbers further decrease as we decrease the safety constant C, as we will discuss below. Figure 2(b) shows the actual fidelity error η_F in those simulations. We confirm that the errors are well below the upper bound (22), especially in late times.

The adaptively chosen step size δt is significantly larger than the one obtained by the error-bound approach. According to Ref. [31], their tight error bound of the second-order product formula gives the possible maximum step size (see Appendix C for more detail)

$$\delta t_{\rm bound} = \left(\frac{\epsilon}{\|[B,[B,A]]\| + \frac{1}{2}\|[A,[B,A]]\|} \right)^{1/3}, \tag{29}$$

for which the difference between $U(\delta t)$ and the second-order Trotterization does not exceed the tolerance ϵ. As shown in Fig. 2(c), the ratio of the adaptively chosen δt to $\delta t_{\rm bound}$ is roughly greater than 10. This means that the step size determined by the error bound tends to be too small for a given tolerance, and the adaptive step size is significantly larger. This discrepancy derives from the fact that Trotter24 utilizes the quantum state at each time step while the error bound applies to arbitrary states and tends to be too pessimistic.

The C dependence of the algorithm is shown in Fig. 3. For various C ($0.8 \leqslant C \leqslant 1.0$), we run the Trotter24 with the other parameters being the same as in Fig. 2. Over the time interval $t_{\rm ini} = 0.0$ and $t_{\rm fin} = 4.0$, we measure the average of the adopted step size δt and the rejection rate, i.e., the average number of occurrences of $\eta_F^{(24)} > \epsilon$ per each time step. As the left y axis shows, the average step size is nearly proportional to C, as expected from its definition. Meanwhile, the rejection rate increases only slowly as C increases, except for the close vicinity of $C = 1$ ($0.99 \lesssim C \leqslant 1$), where C rapidly increases to exceed unity. If we never mind repeatedly measuring $\eta_F^{(24)}$,

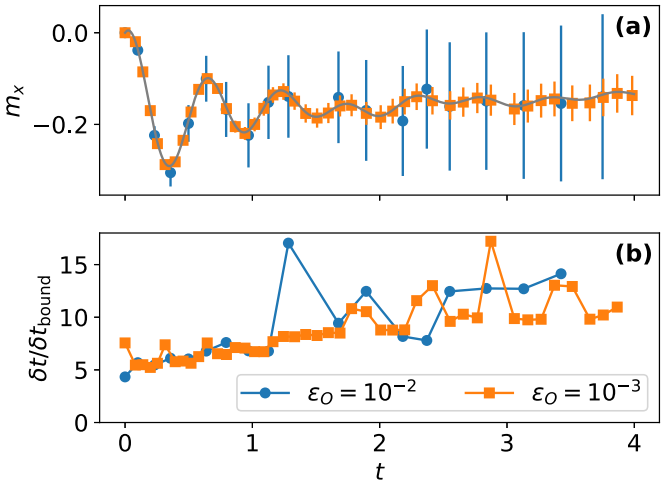

FIG. 4. (a) Dynamics of x-magnetization density m_x under the Hamiltonian (27) calculated by observable-based Trotter24 for $O = m_x$ and tolerance $\epsilon_O = 10^{-2}$ (circle) and 10^{-3} (square). The error bar shows the range where the exact solution resides as indicated by the theoretical upper bound (25). The solid curve shows an accurate solution obtained by a small enough δt, the system size is $L = 18$, and the safety constant is $C = 0.95$. (b) The ratio of the step size δt chosen in each step to $\delta t_{\rm bound}$ obtained by the error-bound approach (29) in the simulations shown in (a).

the choice $C = 1$ is ideal for making δt larger, i.e., the circuit depth shallower. However, by choosing a slightly smaller C, like $C = 0.95$ or 0.90, we benefit from a dramatically reduced rejection rate in exchange for a slight increase in the circuit depth.

Now we implement the observable-based Trotter24 for the same model (27) in the same setup. Suppose again that we are interested in simulating the dynamics of m_x. For this purpose, it is natural to set $O = m_x$, for which the Trotter24 generates Fig. 4. For the smaller tolerance $\epsilon_O = 10^{-3}$, we obtain more accurate results for $\langle\psi(t)|m_x|\psi(t)\rangle$, as expected. As shown in Fig. 4(b), the step size is at least five times larger than $\delta t_{\rm bound}$ given by Eq. (29), whose values are $\delta t_{\rm bound} = 2.31 \times 10^{-2}$ for $\epsilon = 10^{-2}$ and 1.07×10^{-2} for $\epsilon = 10^{-3}$. We note that the exact value always resides within the error bar representing the theoretical upper bound (25). Even when the exact values are not available, the upper bound tells us in what region they are.

Before closing this section, we remark on the stability and efficiency of Trotter24 for simulations over reasonably long times, as seen in Fig. 2(a). This is an advantage over extrapolation methods, such as Richardson's [41], in which physical quantities like $\langle\psi(t)|m_x|\psi(t)\rangle$ are obtained by extrapolating their estimates using different Trotter steps. The extrapolation methods are particularly useful for short times $t \ll 1$ (in units of an inverse local energy scale) because $\langle\psi(t)|m_x|\psi(t)\rangle$ is well approximated by a low-order polynomial in the Trotter steps and allows us to extrapolate the exact solution as the infinite steps limit [42]. For $t \gg 1$, however, the required steps increase significantly, and the estimates with limited steps tend to be unstable due to Runge's phenomenon (see Appendix D for demonstration). Although this pathologic behavior has been addressed using quantum singular value transformations [43], it requires a fault-tolerant quantum computer. When compared under the same gate complexity, Trotter24 is more stable than extrapolation methods, as detailed in Appendix D.

B. Effects of finite $\mathcal{N}_{\rm shots}$

In Sec. V A, we assumed that expectation values are exactly obtained without statistical errors, demonstrating the idealistic behavior of Trotter(m, n). There the only source of error was the Trotter error. In reality, however, the number of available shots (i.e., the number of measurements of circuits) is limited finitely. Thus, in order to guarantee the accuracy of simulations, we need to make sure both the statistical error in the observable evaluation and the Trotter error are within our tolerance. In this subsection we discuss how to implement Trotter(m, n) to control the Trotter error. We consider the same setup as in Sec. V A and aim to estimate $\mathcal{N}_{\rm shots}$ necessary in obtaining the time evolution of $O = m_x$ in the time interval $[t_{\rm ini}, t_{\rm fin}]$ within tolerance ϵ_O.

Before discussing Trotter24, we consider the conventional constant-step (second-order) Trotterization approach. For a fixed step size δt, we compute $|\psi_2(N\delta t)\rangle = T_2(\delta t)^N |\psi_0\rangle$ for an N-step evolution. For each step N, we are computing the desired expectation value

$$\langle\psi_2(N\delta t)|O|\psi_2(N\delta t)\rangle$$

$$= \frac{1}{L}\sum_{j=1}^{L}\langle\psi_2(N\delta t)|\sigma_j^x|\psi_2(N\delta t)\rangle \tag{30}$$

$$= \frac{1}{L}\sum_{j=1}^{L}\langle\psi_2(N\delta t)|H_j\sigma_j^z H_j|\psi_2(N\delta t)\rangle \tag{31}$$

$$= \sum_{\boldsymbol{z}}\frac{1}{L}\sum_{j=1}^{L} z_j P(\boldsymbol{z}) = \frac{1}{L}\sum_{j=1}^{L}\sum_{z_j=\pm1} z_j P_j(z_j), \tag{32}$$

where H_i is the Hadamard gate acting on site j, $P(\boldsymbol{z}) = |\langle\boldsymbol{z}|H_j|\psi_2(N\delta t)\rangle|^2$ denotes the probability of finding $\boldsymbol{z} = (z_1, z_2, \ldots, z_L)$ with $z_j = 1 - 2b_j$ and $b_j = 0, 1$, and $P_j(z_j) = \sum_{\boldsymbol{z}\setminus z_j} P(\boldsymbol{z})$ is the marginal probability for site j. Equation (32) allows us to evaluate the expectation value based on sampling, and the statistical error of estimating the set of marginal probabilities $P_1, \ldots, P_L$ is $\sim\mathcal{N}_{\rm meas}^{-1/2}$ with $\mathcal{N}_{\rm meas}$ being the number of measurements for each time step N. If we take account of the statistical independence among P_j's, the statistical error of $\langle O\rangle$ is reduced to be $\sim(L\mathcal{N}_{\rm meas})^{-1/2}$. Thus, to make sure the estimation error is within the target accuracy with the p-σ confidence interval ($p > 0$), we impose $p(L\mathcal{N}_{\rm meas})^{-1/2} < \epsilon_O$, which means that the minimum required number of measurements is

$$\mathcal{N}_{\rm meas}^0 = \left\lceil \left(\frac{p}{\epsilon_O}\right)^2 \Big/ L \right\rceil, \tag{33}$$

where $\lceil\ldots\rceil$ denotes the ceiling function. For instance, if we demand 2-σ confidence interval for $\epsilon_O = 1\%$, $\mathcal{N}_{\rm meas}^0 = 4 \times 10^4/L$. As shown below, this number is smaller than those for Trotter24 and the adaptive-step (ADA) Trotter [34]. On the other hand, a challenge in the conventional Trotterization is

choosing appropriate step size δt so that the Trotter error is within our tolerance ϵ_O. As discussed in Sec. V, δt, if chosen based on rigorous bounds, tends to be too small, and the number of steps $N_{\rm step} \approx (t_{\rm fin} - t_{\rm ini})/\delta t$ and hence the circuit depth become too large. If one measures $O = m_x$ at every step, the total number of shots becomes $\mathcal{N}_{\rm shots} = N_{\rm step}\mathcal{N}^0_{\rm meas}$.

The number of measurements at each step that Trotter24 requires is twice as large as that the conventional Trotterization does because the Trotter error estimator $\eta_O^{(24)}$ involves two expectation values [see Eq. (10)]. Thus, $\mathcal{N}_{\rm shots} = 2N'_{\rm step}\mathcal{N}^0_{\rm meas}$, where $N'_{\rm step}$ is the number of steps for Trotter24 and tends to be smaller than $N_{\rm step}$. This statistical error contributes to $\eta_O^{(24)}$ by $(2L\mathcal{N}^0_{\rm meas})^{-1/2}\|O\|$, where the factor 2 again takes account of the two expectation values for the second- and fourth-order Trotterizations in $\eta_O^{(24)}$ and the criterion $|\eta_O^{(24)}| < \epsilon_O\|O\|$ should be modified as $|\eta_O^{(24)}| + (2L\mathcal{N}^0_{\rm meas})^{-1/2}\|O\| < \epsilon_O\|O\|$ to guarantee precision within the p-σ confidence interval. Equation (33) simplifies this inequality as

$$|\eta_O^{(24)}| < \left(1 - \frac{1}{\sqrt{2}p}\right)\epsilon_O\|O\|. \tag{34}$$

We note that the formulation reduces to the ideal case in Sec. V A in the limit of $p \to \infty$, where $\mathcal{N}^0_{\rm meas} \to \infty$ and Eq. (34) becomes $|\eta_O^{(24)}| < \epsilon_O\|O\|$.

Figure 5 demonstrates how Fig. 4 changes when we evaluate the expectation values based on sampling with the p-σ confidence interval discussed above. The implementation is the same as in there except for the following two parts. First, the expectation values for the observable and $\eta_O^{(24)}$ are obtained by sampling using Eq. (32) and its counterpart for $|\psi_4(N\delta t)\rangle$ with Eq. (33). Second, the error threshold is replaced by Eq. (34) in the p-dependent way. Note that the error bound (25) is interpreted as the p-σ confidence interval since the error estimation involves statistical errors. The Trotter error tends to decrease as ϵ_O decreases or p increases, although such p dependence is unclear for $t \gtrsim 2$ in $\epsilon_O = 10^{-2}$, where the error bar becomes very large.

The cumulative number of measurements before time t is plotted in Fig. 5(c). Considering Eq. (33) representing the number of measurements at each evaluation of $\eta_O^{(24)}$ and $\langle O\rangle_t$, we have rescaled the number by ϵ_O^{-2} in the plot. Nicely, the number increases in time almost linearly since the rejection rate in finding an optimal δt in each step is kept low. Typical cumulative numbers of measurements for a unit of time $t = 1$ are 10^5 for $\epsilon_O = 10^{-2}$ and 10^7 for $\epsilon_O = 10^{-3}$, which could be achievable in current NISQ devices.

Finally, we discuss the number of measurements required in the ADA Trotter [34], which adaptively chooses δt so that the energy expectation value and variance are close to their ideal values within tolerance. Unlike Trotter24 evaluating O, the ADA needs the expectation values of $H = A + B$ and $H^2 = (A + B)^2$. While $\langle H\rangle_t$ only requires a similar number of measurements to $\langle O\rangle_t$, computing $\langle H^2\rangle_t$ based on sampling is significantly more costly because H^2 is not necessarily local. For example, H^2 involves $AB + BA$, and it contains terms like $\sigma^x_{j'}\sigma^z_j\sigma^z_{j+1}$ $(1 \leqslant j, j' \leqslant L)$. Such terms cannot be simultaneously measured in a single circuit, and one needs multiple, at least $O(L)$, circuits for measurements. Thus, the number of shots required in the ADA Trotter is $O(L)$ greater

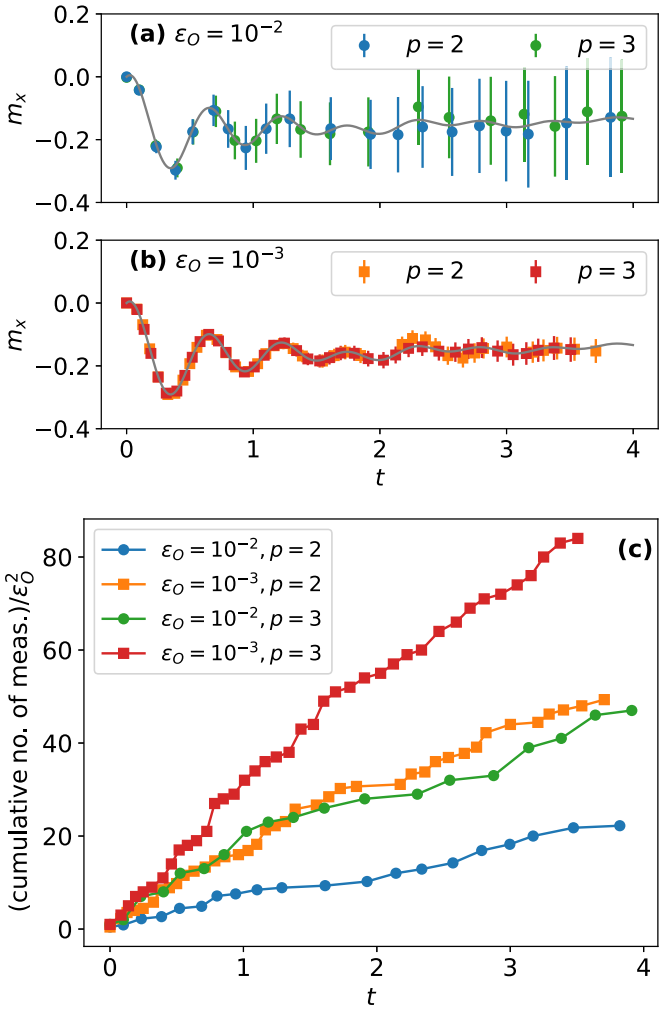

FIG. 5. (a), (b) Dynamics of x-magnetization density m_x under the Hamiltonian (27) calculated by observable-based Trotter24 for $O = m_x$ and tolerance (a) $\epsilon_O = 10^{-2}$ and (b) 10^{-3}, where the expectation values are calculated by sampling with $p = 2$ (circle) and $p = 3$ (square) (see text for detail). The error bar shows the range where the exact solution resides as indicated by the theoretical upper bound (25), which is here interpreted as the p-σ confidence interval. The solid curve shows an accurate solution obtained by a small enough δt, the system size is $L = 18$, and the safety constant is $C = 0.95$. (c) Cumulative number of measurements performed in obtaining (a) and (b) divided by ϵ_O^2.

than that in Trotter24 and the conventional Trotterization. Also, we emphasize again that the tolerance ϵ set for the energy expectation value and variance in the ADA Trotter cannot be translated to the error in the observable O of interest for nonequilibrium states, and the precision guarantee is still elusive, unlike Trotter(m, n).

VI. GENERALIZATION TO TIME-DEPENDENT HAMILTONIANS

Trotter24, developed thus far for time-independent Hamiltonians, is straightforwardly generalized for time-dependent Hamiltonians unlike the previous study [34]. Their study is based on the energy conservation law, which is absent in

time-dependent Hamiltonians, and its generalization to those Hamiltonians is not straightforward and has not been established yet.

Our setup is a generalization of Eq. (1) as

$$H(t) = A(t) + B(t), \tag{35}$$

and we consider approximating the exact evolution $|\psi(t+\delta t)\rangle = U(t,\delta t)\,|\psi(t)\rangle$ for $U(t,\delta t) = \mathcal{T}\exp(-i\int_t^{t+\delta t} H(s)ds)$, where $\mathcal{T}$ denotes the time ordering. Assuming that the quantum state $|\psi(t)\rangle$ at time t is known, we try to approximate the subsequent time evolution for a step size δt by the so-called midpoint rule

$$|\psi_2(t+\delta t)\rangle = T_2(t,\delta t)\,|\psi(t)\rangle\,, \tag{36}$$

$$T_2(t,\delta t) \equiv e^{-iA(t+\delta t/2)\frac{\delta t}{2}} e^{-iB(t+\delta t/2)\delta t} e^{-iA(t+\delta t/2)\frac{\delta t}{2}}. \tag{37}$$

The midpoint rule is known to be a second-order formula, and the fidelity error η_F and the observable error η_O are as small as $O(\delta t^3)$, like in the time-independent-Hamiltonian cases.

To measure the errors in the leading order without using the exact state $|\psi(t+\delta t)\rangle$, we use a fourth-order Trotterization formula for time-dependent Hamiltonians. Focusing on a special case where $A(t) = a(t)A$ and $B(t) = b(t)B$ with $a(t)$ and $b(t)$ are scalars, we utilize the minimum fourth-order Trotterization formula [44]

$$|\psi_4(t+\delta t)\rangle = T_4(t,\delta t)\,|\psi(t)\rangle\,, \tag{38}$$

$$T_4(t,\delta t) \equiv e^{(\frac{s\beta_1}{2}-u)A} e^{s\beta_2 B} e^{\frac{1-s}{2}\beta_1 A} e^{(1-2s)\beta_2 B} e^{\frac{1-s}{2}\beta_1 A} e^{s\beta_2 B} e^{(\frac{s\beta_1}{2}+u)A} \tag{39}$$

consisting of seven exponentials, where $\beta_1 = \int_t^{t+\delta t} a(s)ds$, $\beta_2 = \int_t^{t+\delta t} b(s)ds$, and $\beta_{12} = \frac{1}{2}\int_t^{t+\delta t} dt_2 \int_t^{t_2} dt_1 [b(t_2)a(t_1) - a(t_2)b(t_1)]$, and $u \equiv \beta_{12}/\beta_2$ is assumed to be $O(\delta t^2)$. For more general $A(t)$ and $B(t)$, one can utilize the fourth-order Suzuki formula [22] consisting of 15 exponentials. We can define $\eta_F^{(24)}$ and $\eta_O^{(24)}$ similarly to the case of time-independent Hamiltonians and confirm that $\eta_F \approx \eta_F^{(24)}$ and $\eta_O \approx \eta_O^{(24)}$ in their leading orders.

The algorithms of Trotter24 for time-dependent Hamiltonians are obtained by the replacements $T_2(\delta t) \to T_2(t,\delta t)$ and $T_4(\delta t) \to T_4(t,\delta t)$ in Algorithms 1 and 2. Even though the time-ordered exponential $\mathcal{T}$ exp complicates the propagator $U(t,\delta t)$ for time-dependent Hamiltonians, Trotterizations $T_2(t,\delta t)$ and $T_4(t,\delta t)$ tailored for these cases correctly approximate it as $U(t,\delta t) = T_2(t,\delta t) + O(\delta t^3)$ and $U(t,\delta t) = T_4(t,\delta t) + O(\delta t^5)$. The algorithms of Trotter24 are thus straightforwardly applied to time-dependent Hamiltonians because the complication due to the time dependence is appropriately taken care of by Trotterization formulas.

Let us now implement Trotter24 in an example time-dependent Hamiltonian. Our model is a generalization of Eq. (27) as

$$H(t) = tA + B, \tag{40}$$

where A and B are given in Eq. (27). Although this Hamiltonian is linear in t, Trotter24 equally applies to nonlinear ones. We take the same initial state as in Sec. V and set the time interval as $t_{\rm ini} = -3.0$ and $t_{\rm fin} = +3.0$. Here we only demonstrate the observable-based one since the fidelity-based one works similarly. Figure 6 shows the x-magnetization density dynamics obtained by Trotter24 for different tolerance $\epsilon_O = 10^{-2}$ and 10^{-3}. Like in the time-independent case, Trotter24 provides the dynamics in a precision-guaranteed way, in which the exact solution resides in the error bars given by the preset tolerance ϵ_O.

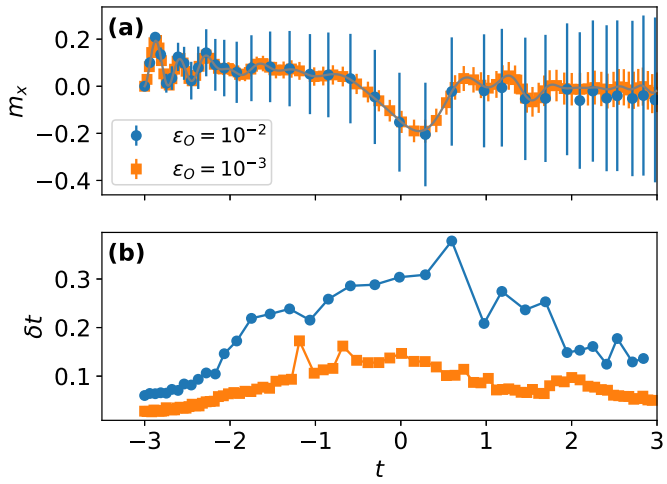

FIG. 6. (a) Dynamics of x-magnetization density m_x under the time-dependent Hamiltonian (40), calculated by observable-based Trotter24 for $O = m_x$ and tolerance $\epsilon_O = 10^{-2}$ (circle) and 10^{-3} (square). The error bar shows the theoretical upper bound (25). The solid curve shows an accurate solution obtained by the fourth-order Trotterization with $\delta t = 10^{-2}$, the system size is $L = 18$, and the safety constant is $C = 0.95$. (b) Step size δt chosen adaptively in the algorithm in each step. Different symbols correspond to those in (a).

Unlike in the time-independent case, the step size tends to decrease as $|t|$ increases, as shown in Fig. 6(b). This is consistent with the fact that the Hamiltonian (40), or the energy scale, is proportional to t when $|t| \gg 1$, for which the step size needs to be decreased to keep the error below the tolerance. Trotter24 automatically chooses the appropriate step size, depending on the instantaneous Hamiltonian as well as the instantaneous quantum state.

VII. CONCLUSIONS AND DISCUSSIONS

We have developed a method of measuring the Trotter error by combining it with another higher-order Trotterization without ancillary qubits. Using this, we devised an algorithm named Trotter (m,n) for Hamiltonian simulations, during which the step size δt is adaptively chosen as large as possible within an error tolerance we set in advance. In each time step, the precision is guaranteed in the sense of Eqs. (22) and (25) with higher-order corrections being neglected. Our algorithm applies to both time-independent and -dependent Hamiltonians, as we benchmarked in the example Hamiltonians in the quantum spin chain mainly for Trotter24, i.e., the case of $(m,n) = (2,4)$. Another merit of Trotter24 is the efficiency in finding the optimal step size δt. According to the benchmark, the estimated δt is rejected less than once on average during each time step by setting the safety constant $C \leqslant 0.99$. In exchange for conducting measurements in each

step, Trotter24 adaptively finds almost the largest δt, which was about 10 times as large as that inferred from the upper bound arguments. Thus, this algorithm keeps the circuit significantly shallower within our error tolerance ϵ.

Although we focused on applying Trotter(m, n) to quantum computers, this algorithm also applies to classical computations. Beyond the system sizes accessible with the full exact diagonalization of Hamiltonians, Trotterization-based algorithms, such as the time-evolution block decimation [45] and the full state-vector evolution [8], are useful on high-performance computers. When we use an mth-order Trotterization, one may want to estimate its error and guarantee that the error is within a tolerance ϵ. For such a purpose, Trotter (m, n) provides these classical computations with a precision-guaranteed adaptive step-size method, enabling reliable simulations for quantum many-body dynamics, although there could be other possible methods.

We have neglected the statistical error in measuring the Trotter error through sampling and the device error inherent to NISQ computers. These errors are, in principle, estimated from the available number of measurements and the device assessment. Also, the error mitigation technique [41,46] helps to reduce these errors, as demonstrated on a 100-qubit-scale NISQ computer [24]. If these errors are below our tolerance and the Trotter error is the bottleneck, Trotter24 will benefit us in optimizing Trotterization in a precision-guaranteed manner. We leave real-device implementations for future work.

ACKNOWLEDGMENTS

Fruitful discussions with H. Zhao, J. Ostmeyer, and K. Mizuta are gratefully acknowledged. T.N.I. was supported by JST PRESTO Grant No. JPMJPR2112 and by JSPS KAKENHI Grant No. JP21K13852. A part of numerical calculations have been performed using Qulacs [47]. This work is supported by MEXT Quantum Leap Flagship Program (MEXTQLEAP) Grants No. JPMXS0118067394 and No. JPMXS0120319794, and JST COI-NEXT program Grant No. JPMJPF2014.

APPENDIX A: SCALINGS OF TROTTER ERRORS

1. Leading-order expression for η_F

According to the Baker–Campbell–Hausdorff (BCH) formula, we have

$$U(\delta t)^\dagger T_m(\delta t) = e^{iH\delta t} e^{-iH\delta t + \Upsilon_{m+1}} = e^{\tilde{\Upsilon}_{m+1}}, \tag{A1}$$

where $T_m(\delta t)$ denotes an mth-order Trotterization and

$$\tilde{\Upsilon}_{m+1} = \Upsilon_{m+1} + [iH\delta t, \Upsilon_{m+1}] + \cdots = \Upsilon_{m+1} + O(\delta t^{m+2}) \tag{A2}$$

is an anti-Hermitian operator, and we used $\Upsilon_{m+1} = O(\delta t^{m+1})$. Thus, we have

$$\begin{aligned}
|\langle\psi(t+\delta t)|\psi_m(t+\delta t)\rangle|^2 &= |\langle\psi(t)|e^{\tilde{\Upsilon}_{m+1}}|\psi(t)\rangle|^2 && \text{(A3)}\\
&= |\langle\psi(t)|\big[1 + \tilde{\Upsilon}_{m+1} + \tfrac{1}{2}\tilde{\Upsilon}_{m+1}^2 + O(\delta t^{3(m+1)})\big]|\psi(t)\rangle|^2 && \text{(A4)}\\
&= 1 + \langle\psi(t)|\tilde{\Upsilon}_{m+1}^2|\psi(t)\rangle + |\,\langle\psi(t)|\tilde{\Upsilon}_{m+1}|\psi(t)\rangle\,|^2 + O(\delta t^{3(m+1)}) && \text{(A5)}\\
&= 1 - \langle\psi(t)|(i\tilde{\Upsilon}_{m+1})^2|\psi(t)\rangle + \langle\psi(t)|(i\tilde{\Upsilon}_{m+1})|\psi(t)\rangle^2 + O(\delta t^{3(m+1)}) && \text{(A6)}\\
&= 1 - \langle\psi(t)|(i\Upsilon_{m+1})^2|\psi(t)\rangle + \langle\psi(t)|(i\Upsilon_{m+1})|\psi(t)\rangle^2 + O(\delta t^{2m+3}), && \text{(A7)}
\end{aligned}$$

where we used $\mathrm{Re}\,\langle\psi(t)|\tilde{\Upsilon}_{m+1}|\psi(t)\rangle = 0$ (since $\tilde{\Upsilon}_{m+1}$ is anti-Hermitian) and Eq. (A2). Therefore, we obtain

$$\eta_F = \sqrt{\langle\psi(t)|(i\Upsilon_{m+1})^2|\psi(t)\rangle - \langle\psi(t)|(i\Upsilon_{m+1})|\psi(t)\rangle^2} + O(\delta t^{m+2}). \tag{A8}$$

Notice that the right-hand side is non-negative since $i\Upsilon_{m+1}$ is Hermitian.

2. Fidelity difference between the exact and measurable expressions

Here we study the difference between

$$\chi \equiv \langle\psi(t+\delta t)|\psi_m(t+dt)\rangle\,, \tag{A9}$$

$$\chi_{mn} \equiv \langle\psi_n(t+\delta t)|\psi_m(t+dt)\rangle \tag{A10}$$

and show $\eta_F = \eta_F^{(mn)} + O(\delta t^{n+1})$. We begin by noting

$$\chi - \chi_{mn} = \langle\psi(t)|U^\dagger(\delta t)[1 - U(\delta t)T_n^\dagger(\delta t)]T_m(\delta t)|\psi(t)\rangle\,. \tag{A11}$$

According to the BCH formula, we have

$$U(\delta t)^\dagger T_n(\delta t) = e^{iH\delta t} e^{-iH\delta t + \Upsilon_{n+1}} = e^{\tilde{\Upsilon}_{n+1}}, \tag{A12}$$

where

$$\tilde{\Upsilon}_{n+1} = \Upsilon_{n+1} + [iH\delta t, \Upsilon_{n+1}] + \cdots = O(\delta t^{n+1}) \tag{A13}$$

is an anti-Hermitian operator, and we used $\Upsilon_{n+1} = O(\delta t^{n+1})$. Thus, we have

$$\chi - \chi_{mn} = \langle\psi(t)|U^\dagger(\delta t)\tilde{\Upsilon}_{n+1}T_m(\delta t)|\psi(t)\rangle + O(\delta t^{2(n+1)}) \tag{A14}$$

$$= \langle\psi(t)|T_m^\dagger(\delta t)\tilde{\Upsilon}_{n+1}T_m(\delta t)|\psi(t)\rangle + O(\delta t^{m+n+2}), \tag{A15}$$

where we used $U(\delta t) = T_m(\delta t) + O(\delta t^{m+1})$ and $\tilde{\Upsilon}_{n+1} = O(\delta t^{n+1})$. Since $\tilde{\Upsilon}_{n+1}$ is anti-Hermitian,

$$\delta\chi \equiv \langle\psi(t)|T_m^\dagger(\delta t)\tilde{\Upsilon}_{n+1}T_m(\delta t)|\psi(t)\rangle = O(\delta t^{n+1}) \tag{A16}$$

is pure imaginary.

Now we rewrite η_F using χ_{mn} as follows:

$$\eta_F^2 = 1 - |\chi|^2 = 1 - |\chi_{mn} + \delta\chi|^2 \tag{A17}$$

$$= 1 - |\chi_{mn}|^2 - (\chi_{mn}^* \delta\chi + \text{c.c.}) + O(\delta t^{2(n+1)}). \tag{A18}$$

Here we note

$$\chi_{mn} = \langle\psi(t)|T_n(\delta t)^\dagger T_m(\delta t)|\psi(t)\rangle \tag{A19}$$

$$= \langle\psi(t)|[T_n(\delta t)^\dagger U(\delta t)][U^\dagger(\delta t)T_m(\delta t)]|\psi(t)\rangle \tag{A20}$$

$$= \langle\psi(t)|e^{-\tilde{\Upsilon}_{n+1}} e^{\tilde{\Upsilon}_{m+1}}|\psi(t)\rangle \tag{A21}$$

$$= 1 + \langle\psi(t)|\tilde{\Upsilon}_{m+1}|\psi(t)\rangle + O(\delta t^{n+1}), \tag{A22}$$

where we used Eqs. (A1) and (A12) to have Eqs. (A21), and (A13) to obtain Eq. (A22). Substituting Eq. (A22) and using the facts $\text{Re}\delta\chi = 0$, $\delta\chi = O(\delta t^{n+1})$, and $\tilde{\Upsilon}_{m+1} = O(\delta t^{m+1})$, we obtain

$$\eta_F^2 = 1 - |\chi_{mn}|^2 + O(\delta t^{m+n+2}), \tag{A23}$$

$$\eta_F = \eta_F^{(mn)} + O(\delta t^{n+1}), \tag{A24}$$

where we used $\eta_F^{(mn)} = O(\delta t^{m+1})$.

3. Observable difference between the exact and fourth-order expressions

Here we show

$$\eta_O - \eta_O^{(mn)} = O(\delta t^{n+1}). \tag{A25}$$

This is simply obtained from

$$\langle\psi_n(t+\delta t)|O|\psi_n(t+\delta t)\rangle$$

$$= \langle\psi(t)|e^{iH\delta t - \Upsilon_{n+1}} O e^{-iH\delta t + \Upsilon_{n+1}}|\psi(t)\rangle \tag{A26}$$

$$= \langle\psi(t)|e^{iH\delta t} e^{-\Upsilon_{n+1}} O e^{\Upsilon_{n+1}} e^{-iH\delta t}|\psi(t)\rangle + O(\delta t^{n+2}) \tag{A27}$$

$$= \langle\psi(t+\delta t)|O|\psi(t+\delta t)\rangle - \langle\psi(t)|[\Upsilon_{n+1}, O]|\psi(t)\rangle + O(\delta t^{n+2}) \tag{A28}$$

$$= \langle\psi(t+\delta t)|O|\psi(t+\delta t)\rangle + O(\delta t^{n+1}), \tag{A29}$$

which means

$$\eta_O - \eta_O^{(24)} = \langle\psi(t+\delta t)|O|\psi(t+\delta t)\rangle - \langle\psi_4(t+\delta t)|O|\psi_4(t+\delta t)\rangle = O(\delta t^{n+1}). \tag{A30}$$

APPENDIX B: FIDELITY ERROR PROPAGATION

To prove Eq. (22) for a general order m [we obtain a proof of Eq. (22) by setting $m = 2$ in the following argument], we begin by introducing

$$\delta U(\delta t) \equiv T_m^\dagger(\delta t) U(\delta t) - 1 = e^{-\tilde{\Upsilon}_{m+1}(\delta t)} - 1 = O(\delta t^{m+1}), \tag{B1}$$

where we used Eq. (A2) and explicitly showed the δt dependence of $\tilde{\Upsilon}_{m+1}$. Introducing

$$\Gamma_{m+1}(\delta t) \equiv i\tilde{\Upsilon}_{m+1}(\delta t) = O(\delta t^{m+1}), \tag{B2}$$

which is Hermitian, we have

$$\delta U(\delta t) = e^{i\Gamma_{m+1}(\delta t)} - 1 \tag{B3}$$

$$= i\Gamma_{m+1}(\delta t) - \frac{\Gamma_{m+1}(\delta t)^2}{2} + O(\delta t^{3(m+1)}). \tag{B4}$$

Now we define

$$\chi_N \equiv \langle\psi(t_N)|\psi_2(t_N)\rangle\,, \tag{B5}$$

which satisfies

$$\delta F_N \equiv 1 - |\chi_N|^2 = \eta_{F,N}^2. \tag{B6}$$

Then we have

$$\chi_N = \langle\psi_0| \overrightarrow{\prod_{i=0,\ldots,N-1}} \left\{ T_m^\dagger(\delta t)\left[1 + i\Gamma_{m+1}(\delta t_i) - \frac{\Gamma_{m+1}(\delta t_i)^2}{2}\right]\right\} \overleftarrow{\prod_{i=0,\ldots,N-1}} T_m(\delta t_i)\,|\psi_0\rangle \tag{B7}$$

$$= 1 - i\sum_{i=1}^{N} \langle\psi(t_i)|\Gamma_{m+1}(\delta t_i)|\psi(t_i)\rangle - \frac{1}{2}\sum_{i=1}^{N} \langle\psi(t_i)|\Gamma_{m+1}(\delta t_i)^2|\psi(t_i)\rangle - \sum_{1\leqslant i<j\leqslant N} \langle\psi(t_i)|\Gamma_{m+1}(\delta t_i) T_m^\dagger(\delta t_{i+1})\ldots T_m^\dagger(\delta t_j)\Gamma_{m+1}(\delta t_j)|\psi(t_j)\rangle + O(\delta t^{3(m+1)}); \tag{B8}$$

$$\delta F_N = \sum_{i=1}^{N} \langle\psi(t_i)|\Gamma_{m+1}(\delta t_i)^2|\psi(t_i)\rangle + 2\,\text{Re}\left[\sum_{1\leqslant i<j\leqslant N} \langle\psi(t_i)|\Gamma_{m+1}(\delta t_i) T_m^\dagger(\delta t_{i+1})\ldots T_m^\dagger(\delta t_j)\Gamma_{m+1}(\delta t_j)|\psi(t_j)\rangle\right] - \left(\sum_{i=1}^{N} \langle\psi(t_i)|\Gamma_{m+1}(\delta t_i)|\psi(t_i)\rangle\right)^2 + O(\delta t^{3(m+1)}), \tag{B9}$$

where we used $\text{Im}\,\langle\psi(t_i)|\Gamma_{m+1}(\delta t_i)|\psi(t_i)\rangle = 0$. Here we notice that

$$\| T_m(\delta t_j)\ldots T_m(\delta t_i)\Gamma_{m+1}(\delta t_i)\,|\psi(t_i)\rangle - \Gamma_{m+1}(\delta t_j)\,|\psi(t_j)\rangle \|^2 = \langle\psi(t_i)|\Gamma_{m+1}(\delta t_i)^2|\psi(t_i)\rangle + \langle\psi(t_j)|\Gamma_{m+1}(\delta t_j)^2|\psi(t_j)\rangle - 2\,\text{Re}[\langle\psi(t_i)|\Gamma_{m+1}(\delta t_i) T_m^\dagger(\delta t_{i+1})\ldots T_m^\dagger(\delta t_j)\Gamma_{m+1}(\delta t_j)|\psi(t_j)\rangle] \tag{B10}$$

is higher order and negligible in our leading-order calculations, meaning that we can replace $2\,\mathrm{Re}[\langle\psi(t_i)|\Gamma_{m+1}(\delta t_i)T_m^\dagger(\delta t_{i+1})\ldots T_m^\dagger(\delta t_j)\Gamma_{m+1}(\delta t_j)|\psi(t_j)\rangle]$ by $\langle\psi(t_i)|\Gamma_{m+1}(\delta t_i)^2|\psi(t_i)\rangle + \langle\psi(t_j)|\Gamma_{m+1}(\delta t_j)^2|\psi(t_j)\rangle$ neglecting higher-order corrections. By doing so and completing squares, we obtain

$$\delta F_N \approx N\sum_{i=1}^{N}[\langle\psi(t_i)|\Gamma_{m+1}(\delta t_i)^2|\psi(t_i)\rangle - \langle\psi(t_i)|\Gamma_{m+1}(\delta t_i)|\psi(t_i)\rangle^2] + \sum_{1\leqslant i<j\leqslant N}[\langle\psi(t_i)|\Gamma_{m+1}(\delta t_i)|\psi(t_i)\rangle - \langle\psi(t_j)|\Gamma_{m+1}(\delta t_j)|\psi(t_j)\rangle]^2. \tag{B11}$$

We notice again that the second term on the right-hand side of Eq. (B11) is negligible in the leading-order calculation. Recalling Eq. (7), we notice that the first term consists of the leading-order fidelity error in each time step, which is guaranteed to be less than ϵ^2 in the algorithm. Therefore, we finally obtain

$$\delta F_N \lesssim N^2\epsilon^2, \tag{B12}$$

$$\eta_{F,N} \lesssim N\epsilon. \tag{B13}$$

APPENDIX C: ERROR-BOUND APPROACH

Here we apply the exact error bound [31] for our example model, obtaining δt guaranteeing the error is less than our tolerance ϵ. According to Ref. [31], we have the following inequality:

$$\|U(\delta t) - e^{-iA\delta t/2}e^{-iB\delta t}e^{-iA\delta t/2}\| \leqslant W_{A,B}\delta t^3, \tag{C1}$$

where

$$W_{A,B} \equiv \|[B,[B,A]]\| + \tfrac{1}{2}\|[A,[B,A]]\|. \tag{C2}$$

Note that interchanging A and B also leads to

$$\|U(\delta t) - e^{-iB\delta t/2}e^{-iA\delta t}e^{-iB\delta t/2}\| \leqslant W_{B,A}\delta t^3. \tag{C3}$$

If $W_{A,B} < W_{B,A}$, inequality (C1) gives a tighter bound, and one may use the second-order formula $e^{-iA\delta t/2}e^{-iB\delta t}e^{-iA\delta t/2}$ in this order of A and B. Otherwise, one may use $e^{-iB\delta t/2}e^{-iA\delta t}e^{-iB\delta t/2}$ whose error is bounded by inequality (C3).

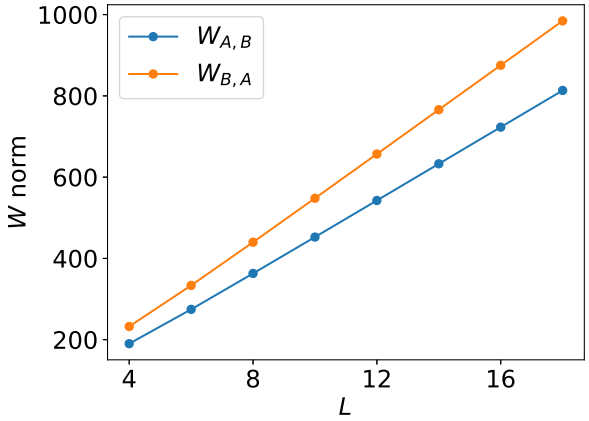

FIG. 7. System-size dependence of the W norms for the example model (27).

The W norms $W_{A,B}$ and $W_{B,A}$ for our example model (27) discussed in the main text are plotted in Fig. 7. Recall that we focused on $e^{-iA\delta t/2}e^{-iB\delta t}e^{-iA\delta t/2}$ in the main text, and this is consistent with the tighter bound (C1) since $W_{A,B} < W_{B,A}$.

The error-bound approach based on the bound (C1) determines δt from

$$W_{A,B}\delta t^3 \leqslant \epsilon. \tag{C4}$$

The possible maximum for δt satisfying this inequality is denoted by $\delta t_{\mathrm{bound}}$ and given in Eq. (29).

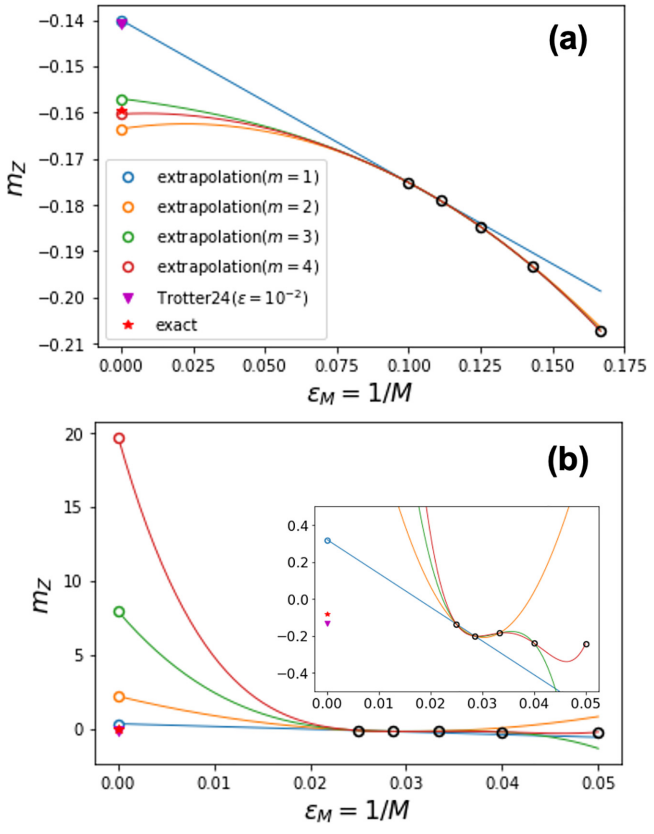

FIG. 8. Comparison between Trotter24 and Richardson's extrapolation at $t_{10} = 1.68$ (a) and $t_{40} = 10.3$ (b). Filled symbols show the magnetization expectation values obtained by the exact calculation (star) and by the observable-based Trotter24 with $\varepsilon = 10^{-2}$. Open black circles show those obtained by the second-order Trotterization, m of which are polynomially extrapolated to estimate the ideal limit $\varepsilon_M \to 0$ (colored circles shown in the legends).

APPENDIX D: COMPARISON WITH RICHARDSON'S EXTRAPOLATION

In this Appendix, we compare Trotter24 and Richardson's extrapolation as follows. We first implement the Trotter24 like in Sec. V to obtain the magnetization expectation values at times t_N ($N = 1, 2, \dots$). On the other hand, for each time t_N, we aim to obtain a good estimate for the exact expectation value using Richardson's extrapolation. Namely, for each integer M taken out of $m+1$ integers, we implement the usual second-order Trotterization with step size t_N/M, having expectation values at t_N. To equate the maximum required gate complexity in both methods, we impose $M \leqslant N$.

Figure 8 shows the comparison at $t = t_{10}$ and t_{40}, where Trotter24 is observable based with $\varepsilon = 10^{-2}$. Figure 8(a) shows results for the shorter $t_{10} = 1.68$. While the accuracy for $m = 1$ is comparable to Trotter24, the extrapolation gives a better estimation as m increases to outperform Trotter24. In contrast, Fig. 8(b) shows the results for the longer $t_{40} = 10.3$, where the extrapolation gives a worse estimation as m increases.

This breakdown of extrapolations for longer times is explained by Runge's phenomenon. The expectation values of O obtained by the second-order Trotterization read as

$$O(t, \varepsilon_M) = \langle \psi(0) \,|\, T_2^\dagger(\varepsilon_M t)^M O T_2(\varepsilon_M t)^M \,|\, \psi(0) \rangle, \tag{D1}$$

where $\varepsilon_M \equiv 1/M$, and we assume that $O(t, \varepsilon_M)$ is $(m+1)$-times differentiable with respect to ε_M. Note that the exact value is given by $O(t, 0) = \langle \psi(0) \,|\, U(t)^\dagger O U(t) \,|\, \psi(0) \rangle = \lim_{M \to \infty} O(t, \varepsilon_M)$. The extrapolation method estimates this by extrapolating an mth-order polynomial curve going through the $(m+1)$ points $(\varepsilon_{M_0}, O(t, \varepsilon_{M_0})), \dots, (\varepsilon_{M_m}, O(t, \varepsilon_{M_m}))$, where we assume $M_0 > \cdots > M_m$. Thus, utilizing the coefficients c_i obtained through Neville's algorithm, we can write the estimate as $\widetilde{O}_m(t, 0) = \sum_{i=0}^m c_i O(t, \varepsilon_{M_i})$. Then, the error of the estimate is bounded as

$$|O(t, 0) - \widetilde{O}_m(t, 0)| \leqslant \max_{0 \leqslant \xi \leqslant \varepsilon_{M_m}} \frac{1}{(m+1)!} \left| \frac{\partial^{(m+1)} O(t, \xi)}{\partial \varepsilon_M^{(m+1)}} \right| \prod_{i=0}^m \varepsilon_{M_i}. \tag{D2}$$

Notice that $\max_{0 \leqslant \xi \leqslant \varepsilon_{M_m}} |\frac{\partial^{(m+1)}}{\partial \varepsilon_M^{(m+1)}} O(t, \xi)|$ can increase when m increases. Consequently, the extrapolation estimates can be worse even though we increase m, and this is known as Runge's phenomenon. This phenomenon can occur when m is too large even if t is short. Generally speaking, $O(t, \varepsilon_M)$ tends to become a more complex function of ε_M as t increases, leading to instability.

Runge's phenomenon is circumvented, in classical numerics, by optimizing the sequence $\varepsilon_0, \varepsilon_1, \dots, \varepsilon_m$ such as the Chebyshev notes. However, this type of optimization is nontrivial in NISQ devices because of the limitation of circuit depth and the constraint that M_i's are integers. In fact, a recent study [43] resorts to a beyond-NISQ quantum computation for solving the optimization. Trotter24 is free from Runge's phenomenon and more stable especially in longer times.

[1] A. W. Harrow and A. Montanaro, Quantum computational supremacy, Nature (London) **549**, 203 (2017).

[2] Y. Cao, J. Romero, J. P. Olson, M. Degroote, P. D. Johnson, M. Kieferová, I. D. Kivlichan, T. Menke, B. Peropadre, N. P. D. Sawaya, S. Sim, L. Veis, and A. Aspuru-Guzik, Quantum chemistry in the age of quantum computing, Chem. Rev. **119**, 10856 (2019).

[3] M. Cerezo, A. Arrasmith, R. Babbush, S. C. Benjamin, S. Endo, K. Fujii, J. R. McClean, K. Mitarai, X. Yuan, L. Cincio, and P. J. Coles, Variational quantum algorithms, Nat. Rev. Phys. **3**, 625 (2021).

[4] A. Aspuru-Guzik, A. D. Dutoi, P. J. Love, and M. Head-Gordon, Simulated quantum computation of molecular energies, Science **309**, 1704 (2005).

[5] S. Lloyd, Universal quantum simulators, Science **273**, 1073 (1996).

[6] J. D. Whitfield, J. Biamonte, and A. Aspuru-Guzik, Simulation of electronic structure Hamiltonians using quantum computers, Mol. Phys. **109**, 735 (2011).

[7] O. Higgott, D. Wang, and S. Brierley, Variational quantum computation of excited states, Quantum **3**, 156 (2019).

[8] T. Jones, S. Endo, S. McArdle, X. Yuan, and S. C. Benjamin, Variational quantum algorithms for discovering Hamiltonian spectra, Phys. Rev. A **99**, 062304 (2019).

[9] W. M. Kirby and P. J. Love, Variational quantum eigensolvers for sparse Hamiltonians, Phys. Rev. Lett. **127**, 110503 (2021).

[10] R. Babbush, J. McClean, D. Wecker, A. Aspuru-Guzik, and N. Wiebe, Chemical basis of Trotter-Suzuki errors in quantum chemistry simulation, Phys. Rev. A **91**, 022311 (2015).

[11] G. H. Low and I. L. Chuang, Optimal Hamiltonian simulation by quantum signal processing, Phys. Rev. Lett. **118**, 010501 (2017).

[12] E. Campbell, Random compiler for fast Hamiltonian simulation, Phys. Rev. Lett. **123**, 070503 (2019).

[13] D. An, D. Fang, and L. Lin, Time-dependent unbounded Hamiltonian simulation with vector norm scaling, Quantum **5**, 459 (2021).

[14] D. An, D. Fang, and L. Lin, Time-dependent Hamiltonian simulation of highly oscillatory dynamics and superconvergence for Schrödinger equation, Quantum **6**, 690 (2022).

[15] A. M. Childs, J. Leng, T. Li, J.-P. Liu, and C. Zhang, Quantum simulation of real-space dynamics, Quantum **6**, 860 (2022).

[16] B. Swingle, G. Bentsen, M. Schleier-Smith, and P. Hayden, Measuring the scrambling of quantum information, Phys. Rev. A **94**, 040302(R) (2016).

[17] J. Zhang, P. W. Hess, A. Kyprianidis, P. Becker, A. Lee, J. Smith, G. Pagano, I.-D. Potirniche, A. C. Potter, A. Vishwanath, N. Y. Yao, and C. Monroe, Observation of a discrete time crystal, Nature (London) **543**, 217 (2017).

[18] K. A. Landsman, C. Figgatt, T. Schuster, N. M. Linke, B. Yoshida, N. Y. Yao, and C. Monroe, Verified quantum information scrambling, Nature (London) **567**, 61 (2019).

[19] L. K. Joshi, A. Elben, A. Vikram, B. Vermersch, V. Galitski, and P. Zoller, Probing many-body quantum chaos with quantum simulators, Phys. Rev. X **12**, 011018 (2022).
[20] A. Y. Kitaev, Quantum measurements and the Abelian stabilizer problem, arXiv:quant-ph/9511026
[21] H. F. Trotter, On the product of semi-groups of operators, Proc. Am. Math. Soc. **10**, 545 (1959).
[22] N. Hatano and M. Suzuki, Finding exponential product formulas of higher orders, in *Quantum Annealing and Other Optimization Methods*, edited by A. Das and B. K. Chakrabarti (Springer, Berlin, 2005), pp. 37–68.
[23] J. Preskill, Quantum computing in the NISQ era and beyond, Quantum **2**, 79 (2018).
[24] Y. Kim, A. Eddins, S. Anand, K. X. Wei, E. van den Berg, S. Rosenblatt, H. Nayfeh, Y. Wu, M. Zaletel, K. Temme, and A. Kandala, Evidence for the utility of quantum computing before fault tolerance, Nature (London) **618**, 500 (2023).
[25] C. Cîrstoiu, Z. Holmes, J. Iosue, L. Cincio, P. J. Coles, and A. Sornborger, Variational fast forwarding for quantum simulation beyond the coherence time, npj Quantum Inf. **6**, 82 (2020).
[26] S.-H. Lin, R. Dilip, A. G. Green, A. Smith, and F. Pollmann, Real- and imaginary-time evolution with compressed quantum circuits, PRX Quantum **2**, 010342 (2021).
[27] Y.-X. Yao, N. Gomes, F. Zhang, C.-Z. Wang, K.-M. Ho, T. Iadecola, and P. P. Orth, Adaptive variational quantum dynamics simulations, PRX Quantum **2**, 030307 (2021).
[28] S. Barison, F. Vicentini, and G. Carleo, An efficient quantum algorithm for the time evolution of parameterized circuits, Quantum **5**, 512 (2021).
[29] R. Mansuroglu, F. Fischer, and M. J. Hartmann, Problem-specific classical optimization of Hamiltonian simulation, Phys. Rev. Res. **5**, 043035 (2023).
[30] Z.-J. Zhang, J. Sun, X. Yuan, and M.-H. Yung, Low-depth Hamiltonian simulation by an adaptive product formula, Phys. Rev. Lett. **130**, 040601 (2023).
[31] I. D. Kivlichan, C. Gidney, D. W. Berry, N. Wiebe, J. McClean, W. Sun, Z. Jiang, N. Rubin, A. Fowler, A. Aspuru-Guzik, H. Neven, and R. Babbush, Improved fault-tolerant quantum simulation of condensed-phase correlated electrons via Trotterization, Quantum **4**, 296 (2020).
[32] A. M. Childs, Y. Su, M. C. Tran, N. Wiebe, and S. Zhu, Theory of Trotter error with commutator scaling, Phys. Rev. X **11**, 011020 (2021).
[33] Q. Zhao, Y. Zhou, A. F. Shaw, T. Li, and A. M. Childs, Hamiltonian simulation with random inputs, Phys. Rev. Lett. **129**, 270502 (2022).
[34] H. Zhao, M. Bukov, M. Heyl, and R. Moessner, Making Trotterization adaptive and energy-self-correcting for NISQ devices and beyond, PRX Quantum **4**, 030319 (2023).
[35] After the submission of our work, Zhao *et al.* [39] publicized their adaptive-step-size Trotterization generalized to time-dependent Hamiltonians.
[36] R. D. Ruth, A canonical integration technique, IEEE Trans. Nucl. Sci. **30**, 2669 (1983).
[37] E. Forest and R. D. Ruth, Fourth-order symplectic integration, Phys. D (Amsterdam) **43**, 105 (1990).
[38] M. Suzuki, Fractal decomposition of exponential operators with applications to many-body theories and Monte Carlo simulations, Phys. Lett. A **146**, 319 (1990).
[39] H. Zhao, M. Bukov, M. Heyl, and R. Moessner, Adaptive Trotterization for time-dependent Hamiltonian quantum dynamics using instantaneous conservation laws, Phys. Rev. Lett. **133**, 010603 (2024).
[40] A. Wisniacki, R. A. Jalabert, H. M. Pastawski, and D. Wisniacki, Loschmidt echo, Scholarpedia **7**, 11687 (2012).
[41] S. Endo, S. C. Benjamin, and Y. Li, Practical quantum error mitigation for near-future applications, Phys. Rev. X **8**, 031027 (2018).
[42] S. Endo, Q. Zhao, Y. Li, S. Benjamin, and X. Yuan, Mitigating algorithmic errors in a Hamiltonian simulation, Phys. Rev. A **99**, 012334 (2019).
[43] G. Rendon, J. Watkins, and N. Wiebe, Improved accuracy for Trotter simulations using Chebyshev interpolation, Quantum **8**, 1266 (2024).
[44] T. N. Ikeda, A. Abrar, I. L. Chuang, and S. Sugiura, Minimum Trotterization formulas for a time-dependent Hamiltonian, Quantum **7**, 1168 (2023).
[45] G. Vidal, Efficient simulation of one-dimensional quantum many-body systems, Phys. Rev. Lett. **93**, 040502 (2004).
[46] Z. Cai, R. Babbush, S. C. Benjamin, S. Endo, W. J. Huggins, Y. Li, J. R. McClean, and T. E. O'Brien, Quantum error mitigation, Rev. Mod. Phys. **95**, 045005 (2023).
[47] Y. Suzuki, Y. Kawase, Y. Masumura, Y. Hiraga, M. Nakadai, J. Chen, K. M. Nakanishi, K. Mitarai, R. Imai, S. Tamiya, T. Yamamoto, T. Yan, T. Kawakubo, Y. O. Nakagawa, Y. Ibe, Y. Zhang, H. Yamashita, H. Yoshimura, A. Hayashi, and K. Fujii, Qulacs: a fast and versatile quantum circuit simulator for research purpose, Quantum **5**, 559 (2021).